EV Traction Control Based on Nonlinear Observers Considering Longitudinal and Lateral Tire Forces

Diego A. Aligia, *Student Member, IEEE*, Guillermo A. Magallan, *Member, IEEE*, and Cristian H. De Angelo, *Senior Member, IEEE*

***Abstract*— An observer-based traction control strategy for electric vehicles is proposed in this paper. The proposed strategy considers the combined effects of lateral and longitudinal traction forces, both for acceleration and regenerative braking, even in curved trajectories. Nonlinear reduced-order observers are designed for estimating tire-road friction condition on each traction wheel and vehicle lateral velocity from which side-slip angles are calculated. A detailed analysis of observers convergence is performed, and a method to know the quality of the estimated variables is also proposed. The proposed traction control strategy allows avoiding the traction wheels skidding during acceleration and braking both in straight trajectories and turning maneuvers. The performance of the proposal is verified through simulation on a complete vehicle model, under different situations and even considering a different vehicle tire model.**

***Index Terms*— Traction control system, combined longitudinal-lateral brush tire model, tire-road friction, nonlinear observer.**

NOMENCLATURE

α	Side-slip angle.
δ	Average steering angle.
ϵ	Observer constant gain.
ω	Angular velocity of the wheel.
$\dot{\omega}$	Angular acceleration of the wheel.
γ	Vehicle yaw rate.
Ψ	Nonlinear transformation.
σ	Tire slip.
a_y	Vehicle lateral acceleration.
C	Parameter dependent on tire characteristics.
d	Vehicle track width.
e	Estimation error.
F	Total force in a tire ($\sqrt{F_x^2 + F_y^2}$).
F_x	Longitudinal force on a tire.
F_y	Lateral force on a tire.
F_z	Normal force on a tire.
$F_{\max}$	Maximum force transmissible to the road.
F_R	Rolling resistance force.
g	Observer constant gain.
i	Subscript used to indicate front ($i = f$) or rear ($i = r$) wheel or axis.
I_w	Wheel spin inertia.
I_z	Inertia respect to the vertical Z axis.
j	Subscript used to indicate left ($j = l$) or right ($j = r$) side.
k_d	Rolling resistance model parameter.
k_s	Rolling resistance model parameter.
l	Distance to center of gravity (CG).
L_μ	Nonlinear gain of the μ_S observer.
L_{v_y}	Nonlinear gain of the v_y observer.
m	Vehicle mass.
μ_S	Tire-road friction coefficient.
R_e	Effective radius of the tire.
v_x	Longitudinal velocity of the center of gravity.
v_y	Lateral velocity of the center of gravity.
T^*	Reference torque.
T_n	Maximum traction motor torque.
T_{rjmax}	Torque saturation calculated by the traction control.

Manuscript received May 20, 2016; revised December 29, 2016 and May 17, 2017; accepted September 15, 2017. This work was supported in part by the National University of Río Cuarto, in part by the Agencia Nacional de Promoción Científica y Tecnológica, and in part by the Consejo Nacional de Investigaciones Científicas y Técnicas. The Associate Editor for this paper was A. Eskandarian. *(Corresponding author: Diego A. Aligia.)*

The authors are with the Grupo de Electrónica Aplicada, Universidad Nacional de Río Cuarto, Río Cuarto X5804BYA, Argentina, and also with the Consejo Nacional de Investigaciones Científicas y Técnicas, Buenos Aires C1033AAJ, Argentina (e-mail: d.aligia.ar@ieee.org).

Color versions of one or more of the figures in this paper are available online at http://ieeexplore.ieee.org.

Digital Object Identifier 10.1109/TITS.2017.2758343

I. INTRODUCTION

IN ELECTRIC Vehicles (EV), the possibility of controlling wheel torque almost instantaneously [1] enables the implementation of different Traction Control (TC) strategies. In addition, electric motors can be used as regenerative brake, which allows recharging batteries and using the TC system as Anti-lock Braking System (ABS), improving energy recovery during braking [2].

Several TC strategies are available in literature. The *Model Following Control* is proposed in [3], where the dynamics of the wheel is treated as a variable-inertia system, assuming that a greater wheel slip can be seen as a lower inertia. This dynamic system is compared with the nominal plant, and the error between them is used to limit the torque applied by the traction motors, in order to maintain the adhesion between the wheel and the road. In the *Optimal Slip Ratio Control* [4], the single wheel slip is regulated in a desired range by controlling the gradient ($\frac{\partial \mu}{\partial slip}$). This control strategy maintains the value of the friction coefficient slope (e.g. positive slope) bounded, which ensures the tire operating

in the stable sliding zone. In [5], an online search method of the optimal operation point of the traction wheels is proposed without the need to measure or calculate the slip ratio, in order to avoid the wheel slip in electric vehicles. A second-order sliding mode control strategy is proposed for wheel slip control in [6], in order to maximize the traction forces.

In [7] an EV traction control strategy is presented, which is based on the detection of the maximum transmissible torque, avoiding the evaluation of the inverse of the nonlinear function that relates the friction coefficient with slip. In [8], a nonlinear observer is designed for road condition estimation and the maximum traction force is controlled using dynamic torque saturation. A robust estimation of traction forces is presented in [9] as well as a strategy to control and maintain them within the stable region. Although all these strategies have shown a good performance, they do not analyze the behavior of the proposals during turning maneuvers.

In situations in which acceleration or braking maneuvers are required while the vehicle performs a turning maneuver, an increase of longitudinal slip occurs to reach the required traction/braking forces, but a decrease of lateral forces can also be observed. To compensate this loss of lateral force in order to allow the vehicle to continue with the desired path, the side-slip angle should be increased. Even more, in case of acceleration/braking maneuvers during sharp turns, the traction wheels may skid producing a large decrease in the lateral forces which could eventually lead to loss of the vehicle control. Therefore, the design of a traction control that ensures the vehicle stability on turning maneuvers should take into account the combined effect of the longitudinal and lateral tires forces.

Some TC strategies are based on the knwoledge of the Tire-Road Friction Condition (TRFC), for which different estimation strategies have been proposed based on [10]: a longitudinal vehicle-tire model [11], [12], a lateral model [13], [14] and a combined model [15], [16]. Among these three categories, there are several works that use different TRFC for the two sides of the vehicle, and some others which only estimate an average road condition. Strategies that only use a longitudinal model to estimate TRFC may not work properly in turning maneuvers, and those that are only based on a lateral model may not be appropriate when longitudinal slip is high. Therefore, proposing a TC based on TRFC estimation able to work on both situations is needed in order to ensure the proper operation when both lateral and longitudinal slip exist. In [17], the estimation of lateral and longitudinal traction forces is carried out and a strategy to estimate TRFC is proposed by means of an adaptive observer and a *Burckhardt/Kiencke* tire model able to operate on extreme adherence situations.

For using the TC system in turning maneuvers, it could be also necessary to know the wheels side-slip angles and/or the lateral velocity. Different side-slip estimation strategies based on Extended Kalman filter (EKF) are compared in [18], using a nonlinear force model, but load transfer is not considered, while computational burden of EKF is usually high. Different strategies for estimating wheels side-slip angles are proposed in [19], considering a combined lateral/longitudinal model. A first strategy combines two open loop estimators for obtaining the side-slip angle, one of them based on the model while the other is a kinematic estimation. Both estimations are combined through a weighted sum using a first order filter. The disadvantages of this strategy is that the filter alters the actual side-slip dynamics, the open-loop estimators may suffer from drift due to sensor bias or noise, and the used model introduce errors when forces are in the nonlinear region. The other two methods are based on an EKF and a scaled Kalman filter with model error compensation. The problem with these techniques is their complexity and high computational burden. In [20] lateral velocity is estimated from a combination of an observer based on a bicycle model and a kinematic observer. Side-slip angles are estimated in [21] through a Kalman filter, using the measurements provided by a GPS and a magnetometer.

A new strategy for estimating side-slip angle and TRFC on electric traction vehicles is proposed in this work. This strategy is based on reduced-order nonlinear observers and allows estimating TRFC on each side of the vehicle as well as lateral velocity, both in curved or straight trajectories. The proposed observers allow implementing a traction control strategy by controlling the torque of the individual traction electric motors. Through dynamic saturation of the applied torque on each side, traction and regenerative braking forces are maintained within their stable region, both for straight and curved trajectories.

The proposed TRFC observers are characterized by their fast convergence compared to the lateral and longitudinal vehicle dynamics, and also with other strategies based on Kalman filter. This is an important requisite in order to allow the TC system to react and correct the vehicle dynamics through the electric traction motors. Besides, the proposed observer does not need the real time calculation of inverse matrices. Moreover, in this work a method to evaluate the quality of the estimated TRFC, based on the analysis of the nonlinear observer feedback gain, is also proposed. This information is used to determine when the estimated variables can be used in the traction control strategy.

This paper is organized as follows: in section II, a study of longitudinal and lateral wheel forces is carried out and the corresponding tire model presented. In addition, the vehicle model is described. In section III the allowed maximum torque values for traction motors are deduced, and a scheme of the proposed traction control strategy is presented. The proposed observers for TRFC and side-slip angle are described in section IV. A method to evaluate the quality of the estimated variables is also presented in this section. In section V, the performance of the proposed traction control and observers for different tire-road conditions and risky driving situations are analyzed and verified through simulation results. Finally, in section VI, main results are discussed and conclusions are drawn.

II. System Model

For traction and stability control, different models that represent the tire-road interaction have been used. These models include *Pacejka Magic Formula* [22], LuGre [23], Dugoff [24], and brush models [24], [25], among others. In this work we use the *combined longitudinal-lateral brush model*, which is a semi-empirical, simple and low-cost computational model.

In addition, this model uses fewer parameters than the Pacejka model, to represent the behavior of the tire under study. These characteristics make this model suitable for the estimation of variables related to tire-road interaction [13], [25].

The longitudinal slip, σ_x, is defined as

$$\sigma_x = \begin{cases} \frac{R_e\omega - v_x}{R_e\omega} & \text{for driving} \\ \frac{R_e\omega - v_x}{v_x} & \text{for braking} \end{cases} \quad (1)$$

and the tire lateral slip is defined as

$$\sigma_y = \frac{v_x}{R_e\omega}\tan(\alpha) \quad (2)$$

where v_x is the longitudinal velocity of the center of mass of the vehicle, R_e is the effective radius of the wheel, ω is the angular speed of the wheel and α is the tire side-slip angle.

The traction force according to the *combined longitudinal and lateral brush model* [24, p. 418], is defined as,

$$F = \begin{cases} \mu_S F_z[3\theta\sigma - \frac{1}{3}(3\theta\sigma)^2 + \frac{1}{27}(3\theta\sigma)^3] & \text{if } \sigma < \sigma_m \\ \mu_S F_z & \text{if } \sigma \geq \sigma_m \end{cases} \quad (3)$$

where $\sigma = \sqrt{{\sigma_x}^2 + {\sigma_y}^2}$, $\theta = \frac{C}{3\mu_S F_z}$, $\sigma_m = \frac{1}{\theta}$, C is a lumped parameter which depends of the tire characteristics and F_z is the normal force.

From (3), the components of the lateral and longitudinal forces can be obtained as follows

$$F_x = \frac{\sigma_x}{\sigma}F \quad (4)$$

$$F_y = \frac{\sigma_y}{\sigma}F \quad (5)$$

and it can be seen that F is the resultant of the geometric sum

$$F = \sqrt{{F_x}^2 + {F_y}^2} \quad (6)$$

In the present model, μ_S is the value taken by the friction coefficient once the wheel starts to skid or enters to the unstable slip region. It is defined as the ratio between the maximum force transmissible to the road for a given road condition and normal force,

$$\mu_S = \frac{F_{\max}}{F_z} \quad (7)$$

Therefore, μ_S is called tire-road friction coefficient (TRFC) and it identifies a particular road condition.

In Fig. 1, the lateral force (5) is represented as a surface $F_y(\sigma_x, \alpha)$ for $\mu_S = 1$ and $F_z = 2500$ N. For different turning maneuvers, F_y will correspond to some point on this surface. As can be appreciated, for a given lateral force transmitted by a tire, when longitudinal slip grows (e.g. due to acceleration in a curved trajectory), side-slip angle must also be increased in order to maintain the same lateral force. Even more, in sudden acceleration during a curve, side-slip angle could reach very high values, which can make the vehicle unstable.

In this situation, the traction control should be able to limit the traction force considering not only the maximum longitudinal force that can be transmitted to the ground due to road adherence, and the normal force (see (7)), but also the lateral force required to perform turning maneuvers.

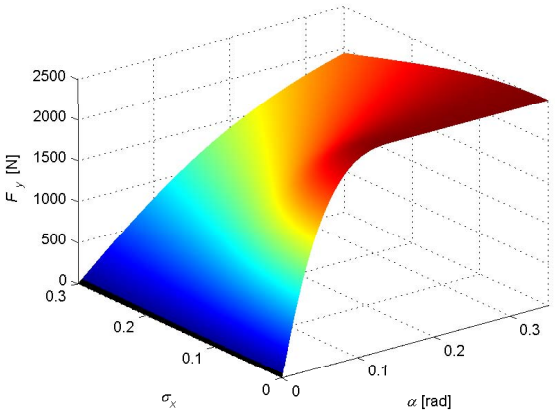

Fig. 1. Lateral force as function of longitudinal slip and side-slip angle.

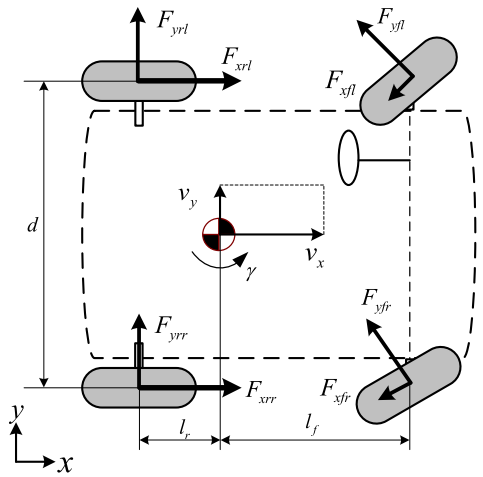

Fig. 2. Vehicle planar model.

For the design of the TC strategy a model of a small EV prototype is considered. This prototype is a rear traction (2WD) four-wheel vehicle with conventional mechanical steering. Vehicle traction is performed by two independently controlled in-wheel electric motors, placed on each rear wheel. Electric motors are driven by variable speed drives able to apply the reference torque in the order of miliseconds, which allows neglecting the dynamics of the actuators [1].

The parameters for this prototype are detailed in Section V. The model considers the planar lateral dynamics and also the rotational dynamics of the traction wheels.

Here, by approximating the steering angles of each wheel by the average between them (δ), the side-slip angles are geometrically calculated as follows [24],

$$\alpha_{fj} = \delta - \arctan\left(\frac{v_y + l_f\gamma}{v_x \mp \gamma\frac{d}{2}}\right) \quad (8)$$

$$\alpha_{rj} = -\arctan\left(\frac{v_y - l_r\gamma}{v_x \mp \gamma\frac{d}{2}}\right) \quad (9)$$

where $j = \{l, r\}$ with l: left, r: right; v_x and v_y are the longitudinal and lateral velocity of the center of gravity (CG), γ is yaw rate, l_f and l_r are the distances from the CG to

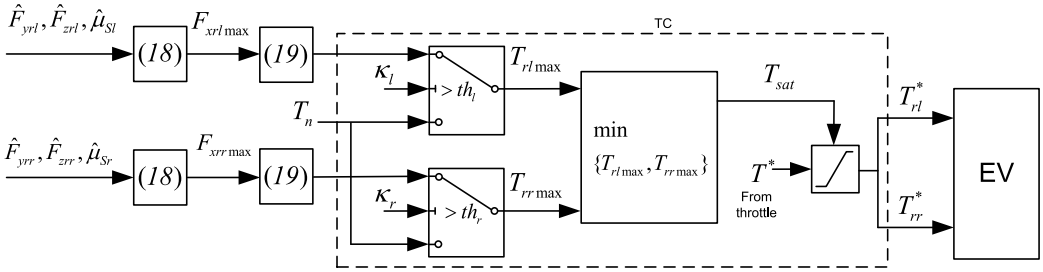

Fig. 3. Proposed traction control scheme.

the front and rear axis, and d is the vehicle track width, respectively.

The lateral forces are calculated individually for each wheel using (5), due to the fact that the TRFC and the normal forces may vary significantly on both sides of vehicle. The force on each axis can be defined as,

$$F_{yf} = F_{yfl}(\alpha_{fl}, \mu_{Sl}, F_{zfl}) + F_{yfr}(\alpha_{fr}, \mu_{Sr}, F_{zfr}) \quad (10)$$

$$F_{yr} = F_{yrl}(\alpha_{rl}, \mu_{Sl}, F_{zrl}) + F_{yrr}(\alpha_{rr}, \mu_{Sr}, F_{zrr}) \quad (11)$$

The model used in this work is then defined by the two equations that represent the lateral planar dynamics of the vehicle,

$$\dot{v}_y = \frac{F_{yf}\cos(\delta) + F_{yr}}{m} - v_x\gamma \quad (12)$$

$$\dot{\gamma} = \frac{F_{yf}\cos(\delta)\,l_f - F_{yr}l_r + (F_{xrr} - F_{xrl})(d/2)}{I_z} \quad (13)$$

where, m is the vehicle mass, I_z is the inertia respect to the vertical axis z and $[(F_{xrr} - F_{xrl})(d/2)]$ is the action of a differential torque (e.g. due to a yaw control action). In addition, the traction wheels dynamics are modeled as follows:

$$\dot{\omega}_{rj} = \frac{1}{I_w}\left(T_{rj} - (F_{xrj} + F_{Rrj})R_e\right) \quad (14)$$

Here, T_{rj} represents the torque applied by the electric motor, F_{xrj} is the traction force modeled by (4), ω_{rj} is the driven wheels angular velocity, F_R the rolling resistance and I_w is the wheel rotational inertia. The rolling resistance, F_R, is modeled as a linear function of the normal force [26],

$$F_{Rrj} = F_{zrj}(k_s + k_d\omega_{rj}R_e) \quad (15)$$

where k_s and k_d are parameters of the friction model and $(\omega_{rj}R_e)$ is the tangential velocity of the tire on the road.

III. Traction Control Strategy

In this paper, a control strategy able to maintain the traction forces within the stable operation region for different road conditions and maneuvers is proposed. This traction control approach is based on the analysis of the total forces (F) exerted by a tire (3) (rear wheels in this particular case). In addition, it ensures good adherence of tires during acceleration and regenerative braking maneuvers in straight and curved trajectories.

Different from previous proposals, we consider that lateral velocity is not measured, but it is estimated using a nonlinear observer. Besides, TRFC on each side of the vehicle are also estimated using nonlinear observers.

A. Calculation of Maximum Applicable Torque

To ensure the operation of the traction control within the stable region of the traction forces, complete slip condition which occurs at ($\sigma >= \sigma_m$), must be avoided. Therefore, according to (7), the maximum force a tire can transmit to the road in any direction is given by,

$$F_{rj_{\max}} = \mu_{Sj}F_{zrj} \quad (16)$$

and the total force on each rear tire is given by:

$$F_{rj} = \sqrt{{F_{xrj}}^2 + {F_{yrj}}^2} \quad (17)$$

In (16) and (17), μ_{Sj}, F_{zrj} and F_{yrj} are imposed conditions dependent on the state of the vehicle. The only action a TC system can take to keep the total force (F) in the stable region, if required, is limiting the longitudinal force by controlling motor torque.

From (16) and (17), the maximum longitudinal force a tire can transmit can be obtained as,

$$F_{xrj_{\max}} = \sqrt{\left(\mu_{Sj}F_{zrj}\right)^2 - F_{yrj}^2} \quad (18)$$

where the lateral force on the tire is calculated from the estimated values of α_r, μ_{Sj} and F_{zrj}, using (5). From the maximum traction force, the maximum applicable torque is calculated by considering (14) at steady state,

$$T_{rj_{\max}} = (F_{xrj_{\max}} + F_{Rrj})R_e \quad (19)$$

The block diagram of the proposed traction control strategy is presented in Fig. 3.

The traction control system input is a torque reference value (T^*), imposed by the throttle position. Reference torque for each wheel is limited through a dynamic saturation to the maximum value, T_{sat}. According to the criteria given in section IV-D, if TC is not needed, torque limit value is set the maximum motor torque T_n.

On the other hand, when TC is needed, T_{sat} is obtained as follows: With estimated $\hat{\mu}_{Sj}$, $\hat{F}_{yrj}$ and $\hat{F}_{zrj}$ values, the maximum torque value that can be applied to each wheel ($T_{rl\ \max}$ and $T_{rr\ \max}$) are calculated. As the maximum torque values on left and right sides may not be equal (e.g. due to different TRFC and different normal forces on one and the other side of the vehicle), the torque reference value is limited

to the minimum value among them. This avoids the appearance of differential torque that may occasionally turn the vehicle unstable.

The output of TC system are the torque references (T_{rl}^* and T_{rr}^*) for each electric motor drive.

Concluding, to implement the proposed control strategy it is necessary to know the TRFC (μ_{Sj}) at each side of the vehicle, the rear lateral forces (F_{yrj}) and the normal forces on the tires (F_{zrj}). Here, the normal forces are estimated according to [27], while TRFC and rear lateral forces are obtained as detailed in the next section.

IV. Estimation of Tire-Road Friction Conditions and Tires Side-Slip Angles

Although the sensors commonly used in vehicular safety systems allow obtaining some information on the longitudinal and lateral dynamics of the vehicle, there are other variables that are difficult or expensive to be measured. Particularly, it becomes necessary to estimate those variables related to TRFC, μ_{Sj}, and the lateral forces, which can be calculated once μ_{Sj} are estimated, as well as the rear side-slip angles, α_{rj}, and normal forces (see (11)).

A new strategy for estimating TRFC on each side of the vehicle as well as the tires side-slip angles using nonlinear reduced-order observers is proposed in this work. These observers are designed from the nonlinear model of lateral and longitudinal forces. The use of nonlinear force models in the observers design provides the advantage that they work properly for maneuvers in which the behavior of forces are significantly away from those of the classical linear bicycle model, particularly on large longitudinal or lateral slip angles and large load transfer.

The following reduced-order observers are proposed for estimating the lateral velocity and TRFC at each side of the vehicle,

$$\dot{\hat{v}}_y = \frac{1}{m}\left(\hat{F}_{yf}\cos(\delta) + \hat{F}_{yr}\right) - v_x\gamma + L_{v_y}(a_y - \hat{a}_y) \quad (20)$$

$$\dot{\hat{\mu}}_{Sl} = L_{\mu_l}(\dot{\omega}_{rl} - \dot{\hat{\omega}}_{rl}) \quad (21)$$

$$\dot{\hat{\mu}}_{Sr} = L_{\mu_r}(\dot{\omega}_{rr} - \dot{\hat{\omega}}_{rr}) \quad (22)$$

where L_{v_y}, L_{μ_l} and L_{μ_r} are state-dependent nonlinear gains to be determined, and $\hat{F}_{yf}$ and $\hat{F}_{yr}$ are the estimated lateral forces given by,

$$\hat{F}_{yf} = F_{yfl}(\hat{\alpha}_{fl}, \hat{\mu}_{Sl}, \hat{F}_{zfl}) + F_{yfr}(\hat{\alpha}_{fr}, \hat{\mu}_{Sr}, \hat{F}_{zfr}) \quad (23)$$

$$\hat{F}_{yr} = F_{yrl}(\hat{\alpha}_{rl}, \hat{\mu}_{Sl}, \hat{F}_{zrl}) + F_{yrr}(\hat{\alpha}_{rr}, \hat{\mu}_{Sr}, \hat{F}_{zrr}) \quad (24)$$

Side-slip angles are obtained from (8)-(9) evaluated on the estimated lateral velocity and the measurements of yaw rate and longitudinal velocity. Besides, a_y is the measured lateral acceleration and

$$\hat{a}_y = \dot{\hat{v}}_y + v_x\gamma, \quad (25)$$

$$\dot{\hat{\omega}}_{rj} = \frac{1}{I_w}\left(T_{rj} - (\hat{F}_{xrj} + \hat{F}_{Rrj})R_e\right) \quad (26)$$

with $\hat{F}_{xrj}$ and $\hat{F}_{Rrj}$ the longitudinal and rolling resistance calculated using the estimated normal forces and TRFCs, and $j = l, r$.

A. Lateral Velocity Observer Design

For obtaining the side-slip angles, α_{ij}, an observer is first proposed for estimating the lateral velocity, v_y. Different from previous proposals, the proposed observer is a reduced-order one, which implies a simpler implementation. Besides, it does not requires operations between matrices or matrix inversions, as in the case of EKF. It is first assumed that the TRFCs (μ_{Sj}) are known, as they are estimated by the observers presented in the next subsection. This condition will be relaxed later, when the convergence analysis of the combined observers is carried out in Appendix A.

This design is based on the lateral velocity dynamics, (12). Considering the following transformation

$$\nu = \Psi_v(v_y, \mu_{Sj}) = a_y = \frac{1}{m}\left(F_{yf}\cos(\delta) + F_{yr}\right) \quad (27)$$

the system in the new coordinates can be expressed as follows,

$$\begin{aligned} \dot{\nu} &= A\nu + \rho(\nu, \mu_{Sj}) \\ y_v &= \nu \end{aligned} \quad (28)$$

where

$$A\nu + \rho(\nu, \mu_{Sj}) = \frac{\partial \Psi_v(v_y, \mu_{Sj})}{\partial v_y}\dot{v}_y$$

Then, the observer (20) in the new coordinates is given by

$$\begin{aligned} \dot{\hat{\nu}} &= A\hat{\nu} + \rho(\hat{\nu}, \hat{\mu}_{Sj}) + g(y_v - \hat{y}_v) \\ \hat{y}_v &= \hat{\nu} \end{aligned} \quad (29)$$

where g is a constant gain that is selected to obtain the desired convergence time (see Appendix A). The observer in the original coordinates becomes,

$$\dot{\hat{v}}_y = \frac{1}{m}\left(\hat{F}_{yf}\cos(\delta) + \hat{F}_{yr}\right) - v_x\gamma + L_{v_y}(a_y - \hat{a}_y) \quad (30)$$

with

$$L_{v_y} = \left(\frac{\partial \Psi_v(v_y, \mu_{Sj})}{\partial v_y}\bigg|_{v_y = \hat{v}_y}\right)^{-1} g$$

Once lateral velocity is estimated, it is possible to calculate the tire side-slip angles from (9) and the corresponding lateral forces from (5) and (3).

B. TRFC Observers Design

These two observers, one for each side of the vehicle ($j = l, r$), are responsible for estimating TRFC on each rear tire. Considering the wheel dynamics (14), and assuming that the TRFC is slowly variable,

$$\dot{\mu}_{Sj} = 0, \quad (31)$$

the following transformation is introduced to design the nonlinear gain,

$$\zeta_j = \Psi_{\mu j}(\mu_{Sj}) = \dot{\omega}_{rj} = \frac{1}{I_w}\left(T_{rj} - (F_{xrj} + F_{Rrj})R_e\right). \quad (32)$$

This transformation makes the output a linear function of the new state, $y_j = \zeta_j$, and

$$\dot{\zeta}_j = \frac{\partial \Psi_{\mu j}(\mu_{Sj})}{\partial \mu_{Sj}}\dot{\mu}_{Sj} = 0. \quad (33)$$

Then, the proposed TRFC observer in ζ coordinates is designed as a reduced order high-gain observer [28], given by

$$\dot{\hat{\zeta}}_j = \frac{1}{\epsilon}\left(y_j - \hat{y}_j\right) = \frac{1}{\epsilon}\left(y_j - \hat{\zeta}_j\right). \tag{34}$$

where ϵ is small enough to make the dynamics of this observers faster than the lateral velocity observer [29]. The reader can refer to Appendix A for a detailed analysis of the convergence of the proposed observers.

Then, in the original coordinates, the proposed observer results

$$\dot{\hat{\mu}}_{Sj} = L_{\mu_j}(\dot{\omega}_{rj} - \dot{\hat{\omega}}_{rj}) \tag{35}$$

with

$$L_{\mu_j} = \left(\left.\frac{\partial \Psi_{\mu j}(\mu_{Sj})}{\partial \mu_{Sj}}\right|_{\mu_{Sj}=\hat{\mu}_{Sj}}\right)^{-1}\frac{1}{\epsilon}. \tag{36}$$

C. Implementation Aspects

As can be noted, the proposed TRFC observer needs the derivatives of the measured wheel angular speed for the correction term. Since a direct computation of this derivative would produce a noisy estimation, the following change of variable is proposed,

$$\dot{\chi}_j = \dot{\hat{\mu}}_{Sj} - L_{\mu_j}\dot{\omega}_{rj} \tag{37}$$

Then the observer is implemented in the substitute variables,

$$\dot{\chi}_j = -L_{\mu_j}\dot{\hat{\omega}}_{rj} = -L_{\mu_j}\frac{1}{I_w}\left(T_{rj} - (\hat{F}_{xrj} + \hat{F}_{Rrj})R_e\right), \tag{38}$$

and the estimated TRFC is calculated as follows,

$$\hat{\mu}_{Sj} = \chi_j + L_{\mu_j}\omega_{rj} \tag{39}$$

Here, motor torque is obtained from the motor controller, while the longitudinal forces are calculated from the measured wheel velocities, the estimated TRFC, and the vehicle longitudinal velocity which is obtained as an average value among those values measured on the undriven front wheels.

The implementation of the proposed observers and the control strategy needs the measurements of the steering angle, lateral acceleration, yaw rate and wheels speed. Steering angle can be measured using a potentiometer or a hall-effect sensor with at least 20 Hz bandwidth and a range of $\pm 25°$. Lateral acceleration and yaw rate measurements can be obtained from an inertial measurement unit (IMU) with a 50 Hz bandwidth. The maximum lateral acceleration to be measured is about ± 1 G while the maximum expected yaw rate is about ± 5 rad/s. The angular wheels speed measurement can be obtained from 1024 pulse/rev. optical encoders, which are also used for the traction motor controller. Finally, the observers can be implemented in a real vehicle using an ARM4 32-bit floating-point microcontroller running at 100 MIPS, discretizing the system with a 4^{th} order Runge Kutta algorithm, with a sampling time of 1 ms.

D. Quality of the Estimated TRFC

A well known problem in the literature is the correct estimation of the TRFC under low slip values [10]. This is due to for low slip values, longitudinal forces are almost a linear function of the slip, being practically independent of μ_S. Due to this problem, under low slip conditions, small disturbances, parameter errors or differences between the model and the real vehicle would cause an incorrect estimation of μ_S. However, this issue does not represent an inconvenience for the control strategy proposed in this work, since for low longitudinal slip conditions, the proposed traction control is not needed (i.e. torque is not limited by (19)).

Despite this, a criteria is needed to evaluate the quality of the estimated variables, in order to know when the estimated TRFC is valid to be used in the calculation of the torque limits. An analysis of the region of convergence of the μ_S observer is performed in [9], while this information is utilized to evaluate the quality of the estimated values for control purposes. The problem of such proposal is that the region of attraction is dependent of the estimated variables.

In the present work, a method for evaluating the quality of the estimated variables independent of such estimations is proposed. The proposal is based on the analysis of the nonlinear gain of the TRFC observer (36). As can be seen, the reciprocal of this term is proportional to the derivative of the longitudinal force with respect to μ_S,

$$\left.\frac{\partial \Psi_{\mu j}(\mu_{Sj})}{\partial \mu_{Sj}}\right|_{\mu_{Sj}=\hat{\mu}_{Sj}} = \frac{\partial \dot{\hat{\omega}}_{rj}}{\partial \hat{\mu}_{Sj}} = -\frac{R_e}{I_\omega}\frac{\partial \hat{F}_{xrj}}{\partial \hat{\mu}_{Sj}} \tag{40}$$

This derivative indicates the degree of dependence of the longitudinal force on the parameter μ_{Sj}, for a given value of σ_x and σ_y. A small value of this derivative means that the longitudinal force is in the linear region, which implies that the estimated value of μ_{Sj} is not reliable, and should not be used for torque limits calculation. On the other hand, if the value of this derivative is high, longitudinal forces are highly dependent of μ_{Sj}, and the estimated values are correct and can be used for torque limiting.

As can be seen in Appendix B, function (40) is negative and it has an absolute minimum in the interval $0 < \sigma_x < \sigma_m$. Besides, the value of this minimum is independent of μ_S, which means that it can always be calculated, independently of the quality of the estimated variables and of the vehicle driving conditions.

According to the vehicle driving and road conditions, different operating region of the proposed observers can be identified, as shown in Table I. Here, different combinations of longitudinal and lateral slip that can be found are considered. For simplicity it is assumed that lateral side-slip on both rear wheels are equal. In the table, "low" means that force is in the linear region, while "high" refers to forces beyond the linear region.

As previously explained, a correct estimation of $\hat{\mu}_{Sj}$ is obtained when forces are beyond the linear region. Therefore, for cases $\langle 1 \rangle$ to $\langle 3 \rangle$ the estimation of $\hat{\mu}_{Sj}$ is not reliable, but traction control is not needed in such cases.

TABLE I
OPERATING OBSERVERS REGIONS

Case	σ_{xrl}	σ_{xrr}	σ_{yrl}	TC needed?	$\hat{\mu}_{Sj}$ - converge?	$\hat{v}_y$ - converge?
1	0	0	0	no	no	don't care
2	low	low	low	no	no	yes
3	low	low	high	no	no	yes
4	low	high	low	right wheel	only right	yes
5	low	high	high	right wheel	only right	yes
6	high	low	low	left wheel	only left	yes
7	high	low	high	left wheel	only left	yes
8	high	high	low	both wheels	both	yes
9	high	high	high	both wheels	both	yes
10	sat	sat	0	both wheels	both	-
11	0	0	sat	no	no	no

Cases ⟨4⟩ to ⟨7⟩ are not usual driving conditions, but they can occur when road condition changes only on one side of the vehicle. In these cases, $\hat{\mu}_{Sj}$ is correctly estimated only on the wheel with high slip, while traction control is only needed in that wheel (i.e. on the side with high slip).

In cases ⟨8⟩ and ⟨9⟩ longitudinal slip is high on both sides, so $\hat{\mu}_{Sj}$ is correctly estimated on both wheels. Such situations require the traction control on both wheels to avoid wheels skidding.

Different from the μ_{Sj} observers, the estimation of $\hat{v}_y$ converges both for the linear region of the forces and beyond it. Then, in cases ⟨2⟩, ⟨4⟩, ⟨6⟩ and ⟨8⟩, lateral velocity is correctly estimated since lateral forces are in the linear region, so they are not dependent on the estimation of $\hat{\mu}_{Sj}$. For cases ⟨3⟩, ⟨5⟩ and ⟨7⟩, the performance of the lateral velocity observer can be slightly affected by the $\hat{\mu}_{Sj}$ which is no properly estimated, producing that the estimation error does not converges to zero, but to a small value. In cases ⟨8⟩ and ⟨9⟩ μ_{Sj} is rightly estimated, and the same occurs with $\hat{v}_y$.

In ⟨10⟩ longitudinal force is saturated (wheels are skidding) and lateral velocity is null. In such case the estimation of both $\hat{\mu}_{Sj}$ is correct. Traction control should avoid to reach this situation.

Finally, ⟨11⟩ represents a case where the vehicle is laterally skidding without control, with null longitudinal slip, while lateral forces are saturated. In this situation μ_{Sj} and lateral velocity are not observable. Even when the observers do not provide a reliable estimation, traction control could not do anything since there is not available longitudinal force.

V. EVALUATION OF THE PROPOSED CONTROL STRATEGY

To verificate the traction control strategy and the observers proposed in this work, simulations were carried out using Simulink/CarSim environments, using a full model of vehicle whose parameters are presented in Table II. The rest of parameters corresponds to a generic class A vehicle, provided by CarSim. The CarSim vehicle model is a multibody dynamic model that considers the effects of suspension, load transfer, aerodynamic force, etc. The tire model used by this simulator includes rolling resistance, camber trust effect, combined slip, dynamic radius variation depending on load variations, and dynamics due to rolling are included using relaxation length for lateral and longitudinal slip [30]. In order to accomplish the desired velocity of convergence, the following observer gains were selected: $g = 10$, $\epsilon = 0.001$. In the first results (V-A to V-C), the tire model used by the simulator is the *combined longitudinal-lateral brush tire model*. Subsequently, for the case V-D, this model is replaced by a Pacejka model in order to verificate the proposal even for significant differences of the tire model. In this work, electric traction motors are considered to be driven by variable speed drives able to apply reference torque in the order of miliseconds [1]. This allows neglecting the dynamics of the actuators.

TABLE II
VEHICLE PARAMETERS

Parameter	Value
Vehicle mass (m)	590 kg
Unsprung mass (m)	80 kg
Distance CG to frontal axis (l_f)	1.02 m
Distance CG to rear axis (l_r)	0.68 m
Vehicle track width (d)	1.4 m
Roll inertia	152 kgm^2
Pitch inertia	356 kgm^2
Yaw inertia (I_z)	352 kgm^2
Wheel inertia (I_w)	1.9 kgm^2
Tire radius (loaded) (r_d)	0.292 m
Tire vertical rigidness	200000 N/m
Tire model lumped parameter (C)	50000 N/rad
Rolling resistance parameter(k_s)	3.610^{-3}
Rolling resistance parameter(k_d)	0.2210^{-3} s/m
Tire lag for F_x	50 mm
Tire lag for F_y	565 mm

A. Observers Convergence

A first test was performed to show the observers convergence, starting with a non-zero estimation error. Two cases are considered in this simulation. In the first case, the vehicle is accelerating with a 500 N force on each traction wheel since $t = 0s$ on a high adherence road ($\mu_S = 0.8$) in a straight path (no lateral velocity). At $t = 2s$ the μ_{Sj} observers are activated with an initial condition ($\mu_{Sj} = 0.2$). and Figs. 4(a) and (b) show the estimation error on ζ coordinates and in the original coordinates, respectively. As can be seen, convergence time is below 10 ms, while a small final error appears on the estimation error of μ_{Sj} due to some model mismatch.

In the second case, the vehicle is turning with a constant steering angle, while accelerating with a 500 N force on each traction wheel on a high adherence road ($\mu_S = 0.8$). Lateral acceleration is 5 $\mathrm{m/s}^2$. TRFC observers are correctly estimating $\hat{\mu}_{Sj}$ while the lateral velocity observer is activated at $t = 2s$ with an initial estimation error.

Fig. 4(c) shows that the estimation error in the ν coordinates converges to zero, while the estimation error on the original coordinates, v_y, goes to a small value close to zero. As can be appreciated, convergence time of this observer is about 300 ms, as expected from the observer design.

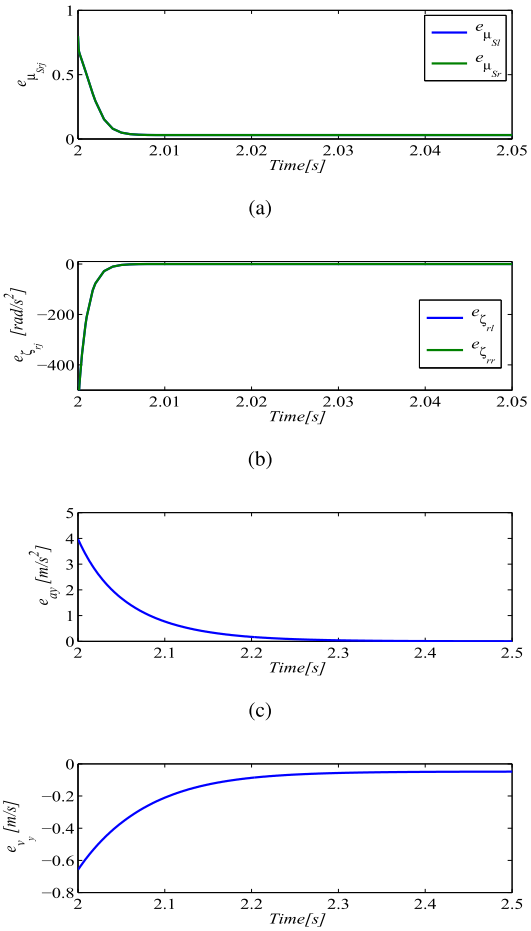

Fig. 4. Estimation errors of: (a) TRFC, μ_{Sj}; (b) ζ; (c) v; and (d) Lateral velocity, v_y.

B. Case 1: ISO7975: Braking on a Curved Trajectory.

In this case the simulated maneuver follows the guidelines given by standard ISO 7975:2006, but adapted to the restriction of the considered vehicle. In this simulation, the vehicle circulates along a straight trajectory with high adherence ($\mu_{Sj} = 0.8$) between $t = 0s$ and $t = 2s$, without acceleration and at an initial velocity of 80 km/h. At $t = 2s$, it begins to turn until a lateral acceleration of 4 m/s^2 is reached (about 125 m turning radius) (see Fig. 5(a)). At $t = 5s$ it brakes suddenly with the rear wheels (regenerative braking) while turning, producing an initial deceleration of -2 m/s^2. It must be noted that even when the standard requires a higher deceleration, such value cannot be achieved due to only the rear wheels are used for braking (regenerative braking only), and due to the load transfer to the front wheels during the maneuver reduces the braking capacity of the rear wheels.

In Fig. 5(b), it can be seen that between $t = 0s$ and $t = 5s$, traction forces stays far from saturation, while between $t = 5s$ and $t = 9s$, they are limited by the traction control to the lower limit value ($F_{xrl_{\max}}$ in this case, due to the load transference to the right side).

From $t = 10.2s$, due to the vehicle velocity decreases, the needed lateral force also decreases, thus increasing the available longitudinal force $F_{xrl_{\max}}$.

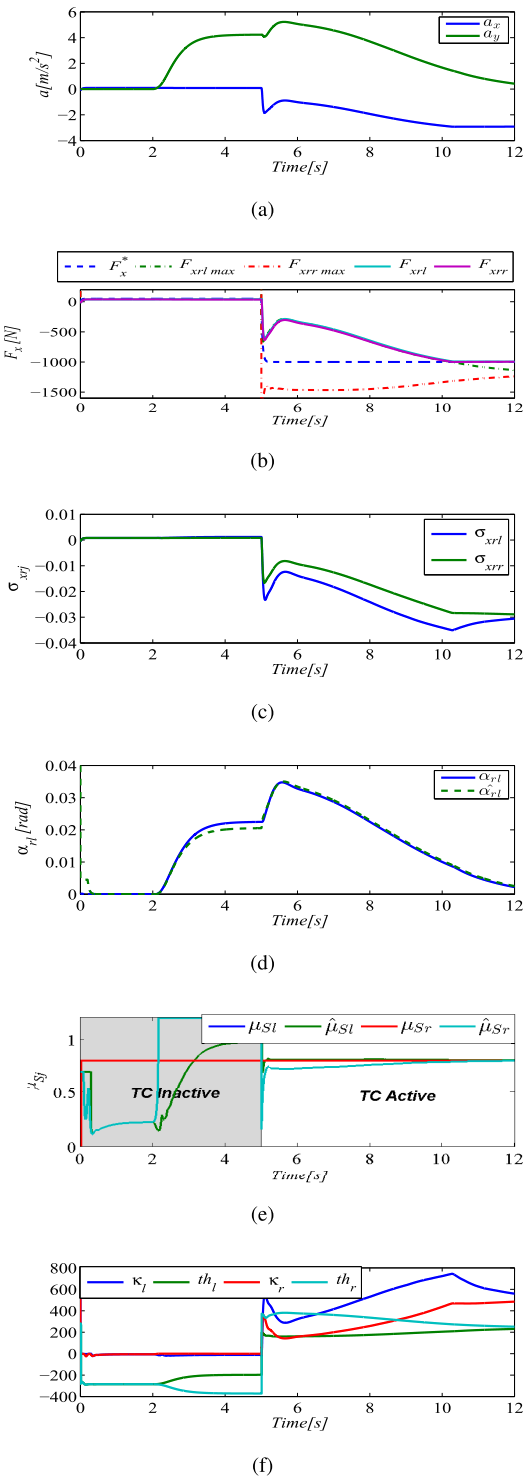

Fig. 5. Case 1. Braking on a curved trajectory. (a) Longitudinal/lateral acceleration. (b) Traction forces. (c) Longitudinal slip. (d) Rear left side-slip angle. (e) Tire-road friction coefficients. (f) Threshold and indicators of quality of $\hat{\mu}_{Sj}$.

Between $t = 0s$ and $t = 5s$, the estimation of μ_{Sj} is not reliable, due the low value of longitudinal slip. As can be seen, in this interval derivatives of the longitudinal forces with respect to μ_{Sj} are below the threshold, $|\kappa_j| < |\text{th}_j|$ (Fig. 5(f)), which indicates that longitudinal forces are slightly dependent of μ_{Sj}, and the traction control is not necessary.

From $t = 5s$ a reliable estimation of TRFC can be appreciated, which coincides with the increase of the force derivatives. Due to the load transference to the right side, the left longitudinal force is closer to its saturation than the right one, which produce that the quality of the estimation of μ_{Sl} is better than μ_{Sr}. The same can be appreciated in the comparison of each force derivative with its corresponding threshold, in Fig. 5(f). Besides, only μ_{Sl} is used to calculate the limit force value, since the limit of the left force ($F_{xrl_{\max}}$) is lower than the one of the right force (see Fig. 5(b)).

Figures 5(c) and 5(d) show that both, longitudinal slip and side-slip angle values are maintained low, ensuring a good adherence.

C. Case 2: Longitudinal Acceleration on a Curved Trajectory and Change of Tire-Road Friction Conditions

Acceleration of the vehicle during a left-turning maneuver was performed in this case. A decrease in adherence is also introduced into one side of the vehicle to demand traction control performance even more. The vehicle travels following a curved trajectory with a 50 km/h initial velocity, on a high adherence surface ($\mu_S = 0.8$). From $t = 2s$, the driver accelerates the vehicle and the traction control produces a 400 N longitudinal traction force to the road. Fig. 6 shows the results obtained using the proposed TC strategy. It can be observed in Fig. 6(a) the comparison between the force required for the maneuver (F_x^*) and the maximum longitudinal forces ($F_{xrl\ max}$ and $F_{xrr\ max}$) the vehicle is capable of transmitting for this situation, obtained from (16).

A change of TRFC to a low adherence surface ($\mu_{Sl} = 0.2$) on the left side of the vehicle is performed at $t = 4\ s$. It is appreciated that from this moment, the estimation of μ_{Sl} converges to the actual value (Fig. 6(d)). The same can be concluded from the comparison of the derivative of the left force with its corresponding threshold ($|\kappa_l| > |\text{th}_l|$), in Fig. 6(e). Also, when the threshold is exceeded, traction control must limit the applied torque. From $t = 4s$, the required longitudinal force is greater than the maximum force the left wheel can transmit, so traction control limits the force on both wheels to the saturation value calculated for the left wheel. Due to the control action, both longitunal slips and side-slip angles remains within stable forces region and the vehicle can continue its trajectory without losing stability, as seen in figures 6(b) and 6(c). Figure 6(c) also shows that the estimated side-slip angle is close to its actual value during the maneuver, except at the beginning, when the applied force is small.

D. Case 3: TC Strategy Test for Changes in the Tire Model

Since the proposed TC strategy is based on observers, and they were designed in base of a particular tire-road force model (combined longitudinal-lateral brush tire model), it is desirable to evaluate its performance when the actual tire-road model (or its parameters) differs from the one considered for the design. With this aim, we compare two cases: when the same tire-road (brush) model is used in the simulated vehicle, and when a Pacejka tire model is used for the vehicle.

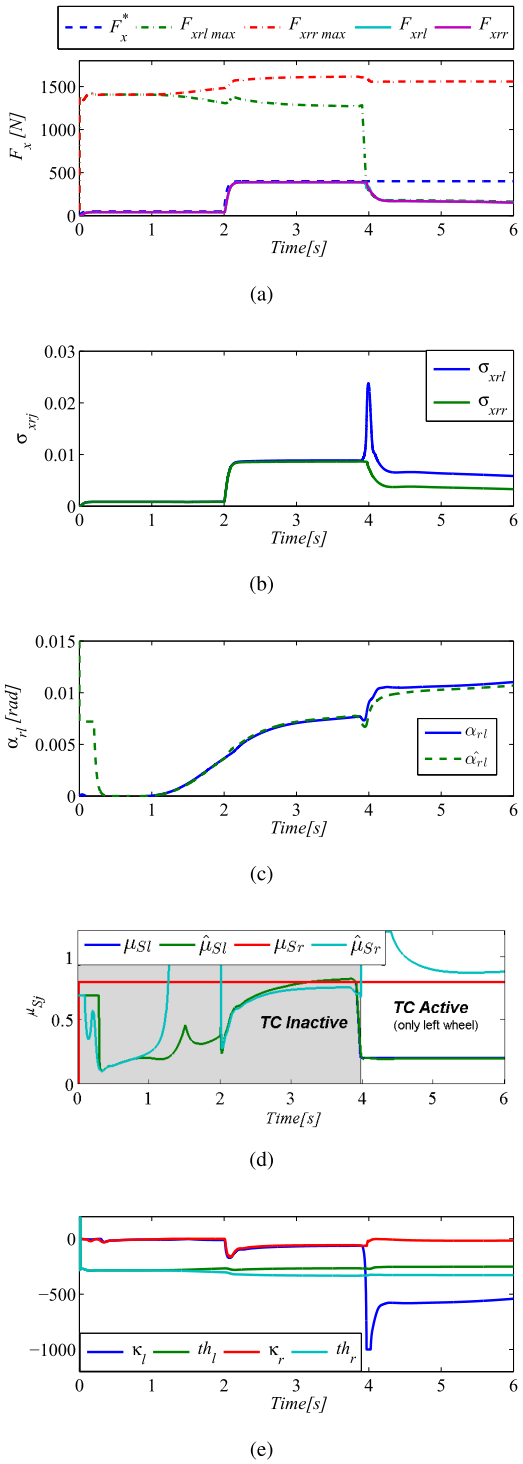

Fig. 6. Case 2. Longitudinal acceleration on a curved trajectory and change of tire-road friction conditions. (a) Traction forces. (b) Longitudinal slip. (c) Rear left side-slip angle. (d) Tire-road friction coefficients. (e) Threshold and indicators of quality of $\hat{\mu}_{Sj}$.

Pacejka model corresponds to a $205/55R16$ tire whose parameters are shown in [31]. Since the parameters of the Pacejka model presented in [31] correspond to an unitary friction-coefficient surface, the similarity method [32] is used here to simulate the behavior of the tire in a less adherent surface. In order to take into account the behavior of the tire during the curve, combined slip theory is used.

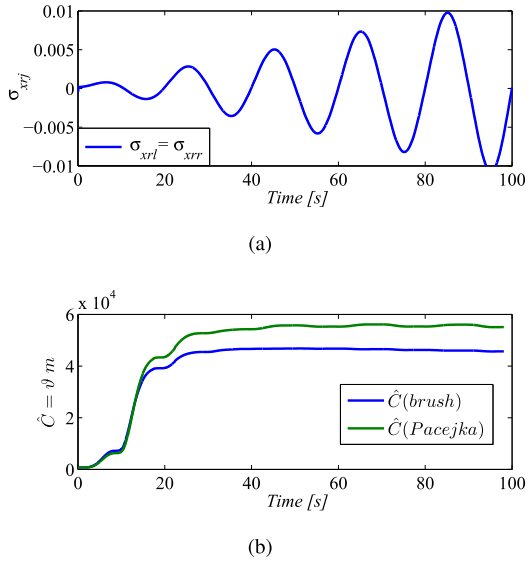

Fig. 7. Case 3a. (a) Longitudinal slip (b) C estimation.

In particular, the *combined longitudinal-lateral brush tire model* in which the proposed strategy is based, is mainly characterized by the parameter C (see (3)). This parameter depends on the physical characteristics of the tire, and it must be identified in an initial commissioning stage. However, it could also change with the tire wear, or when the tire is replaced by a different brand or model.

This parameter (C) models the slope of the longitudinal force for null (or very small) slip values. The observers proposed in this paper are robust to variations of C in the high-slip region because in that region the force is highly dependent on μ_S, but little dependent on the C parameter. However, their performance and the quality of the estimated μ_{Sj} could be better if the value of C represents the actual slope of the force-slip curve. Also, the parameter C is needed for properly evaluating the maximum applicable torque, since it is calculated from the force model.

For this reasons, a recursive estimator is proposed in order to estimate the C parameter of the force model (see Appendix C). This estimation is performed considerably slower than the observers, since changes in C only occur when the tire is changed. Then, this parameter can be considered a known constant, but its estimated value ($\hat{C}$, adjusted by the recursive estimator) is used in the proposed observers.

For this case, two results are presented. First, the behavior of the recursive estimator is demonstrated. Then, the performance of the proposed traction control strategy using the estimated parameter, $\hat{C}$, is shown when a different tire model is used in the vehicle.

The estimation algorithm is tested considering the following maneuver. The vehicle is travelling in a straight trajectory at low longitudinal velocity (36 km/h) during 90 s. Then, a sinusoidal torque reference (with a mean value in order to compensate the vehicle losses) with growing amplitude is applied to both traction motors. This allows producing a variable-growing longitudinal slip, which is limited to the linear force region (Fig. 7(a)). This emulates a driving condition with successive (soft) accelerations and regenerative brakings.

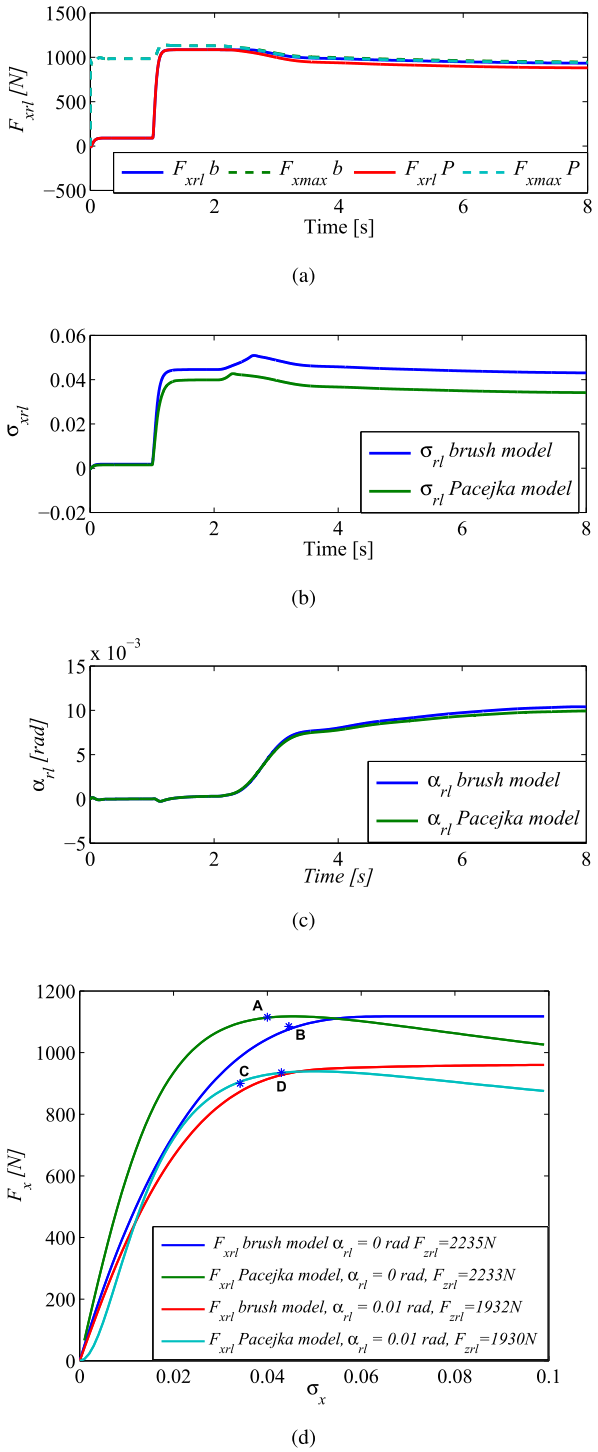

Fig. 8. Case 3b. Comparison for change in the tire model. (a) Traction forces. (b) Longitudinal slip. (c) Rear left side-slip angle. (d) Steady state operating points.

This condition is run twice: first using the brush model with $C = 50\,000$ in the CarSim vehicle model, and then using the previously described Pacejka tire model in the simulated vehicle. The obtained results are shown in Fig. 7(b) where it can be appreciated that a $\hat{C} = 47\,000$ value is obtained for the brush model, while a $\hat{C} = 56\,500$ value is estimated for the Pacejka model.

In both cases, the estimated value corresponds to the slope of the linear approximation of the force model, as modeled in the estimation algorithm (see Appendix C).

Below, the results of the traction control algorithm using the $\hat{C}$ parameters estimated in the previous tests are presented in Fig. 8.

Lets consider the following maneuver: the vehicle is circulating along a straight trajectory with low adherence ($\mu_{Sj} = 0.5$) and at $t = 1$ s the driver accelerates producing a 1200 N reference force. Since the actual TRFC does not allow to apply the reference force to the road, the TC system will limit the traction forces, as seen in Fig. 8(a). Later, the vehicle begins a left-turning maneuver with a constant steering angle, and after about 4 seconds, the rear side-slip angles becomes stable at $\alpha_r = 0.01$ rad (see Fig. 8(c)). Due to the action of lateral load transfer the rear left normal force decrease. The transient behavior of the longitudinal slip for this maneuver is shown in Fig. 8(b).

For the proposed maneuver, two steady state conditions are presented in Fig. 8(d): the first one corresponds to the straight trajectory (at $t = 2$ s), while the second one correspond to the turning condition, once the side slip stabilizes at $\alpha_r = 0.01$ rad (at $t = 8$ s). When the brush model is considered, such conditions correspond to the longitudinal force behavior shown in the blue and red curves of Fig. 8(d), respectively. The TC system limits the longitudinal force, as shown in Fig. 8(a), resulting in the operating points marked as B and D, respectively. In point D, the longitudinal force decrease for two reasons: the increase in the lateral force and the decrease in the normal force due to load transfer on the curve. As it can be appreciated, in both cases the TC system avoids the increase of longitudinal slip (Fig. 8(b)), maintaining the forces in the stable region.

When the Pacejka model is used in the vehicle, the longitudinal force behavior corresponds to the green and sky blue curves of Fig. 8(d), for the straight and curve trajectory, respectively. In this case, the operating point due to the action of the TC system corresponds to points A and C. It can be appreciated that even when the model is different from the one used for the observer design, the TCS is still able to maintain the tire in the stable region, both in the straight and curve trajectory.

VI. Discussion and Conclusions

A new strategy for estimating side-slip angles and tire-road friction condition on both sides of the vehicle was proposed in this paper. The estimation strategy is based on nonlinear reduced-order observers. A traction control strategy which limits the applied traction forces based on the estimated variables is also proposed. This strategy allows keeping the traction and regenerative braking forces within its stable region, both for straight and curved trajectories.

The proposed strategy controls the maximum traction torque to maintain the tire forces in the stable region.

To accomplish this, two nonlinear reduced-order observers were proposed for the estimation of the tire-road friction condition at each side of the vehicle, and lateral velocity. For the design of observers and the calculation of torque limitations, *the combined longitudinal-lateral brush tire model* was used, whose main characteristic is its simplicity compared with other more complex models.

A method for identifying the quality of the estimated variables was also presented. An indicator independent of both, the estimated variables and the driving and road conditions was determined. This indicator allows determining the quality of the estimated variables and when they must be used in the traction controller to limit the applied forces. A recursive estimator was proposed in order to estimate the value of the parameter C involved in the force model, used in the designed observers. This makes the proposal more robust in front of uncertainties in the tire model, which improves the performance of the traction control strategy.

Compared with some previous proposals, the following differences can be highlighted. The proposed reduced-order observers provide a faster convergence of the estimated TRFC, when compared to the strategy presented in [25]. Besides, in [25] the lateral velocity is assumed known (or estimated by another method), without considering its influence on the estimation of the TRFC. Instead, in the present paper convergence of the combined observers is ensured, while the improvement in the convergence time of the TRFC estimation allows implementing a traction control which can react to sudden changes of road condition.

In [13] TRFC and side-slip angle is also estimated using nonlinear observers, however, only lateral dynamics is considered. Instead, in the present proposal the observer convergence is guaranteed also in maneuvers involving longitudinal slip during curves, which allows implementing a traction control strategy during acceleration or braking, both in straight or curved trajectories. Besides, in our work self-aligning torque measurement is not needed, but wheel angular speed must be measured.

Both the traction control and the observers were verified for different operation conditions using a Simulink/CarSim environment with a complete vehicle model.

In a first case the behavior of the proposed observer-based traction control strategy was evaluated following the guidelines of standard ISO7975. The performance of the traction control was analyzed for a sudden braking maneuver during a turning maneuver. This situation is more critical even for acceleration, provided that during braking, normal loads on the rear wheels decrease and so does its road adherence capability. A stable vehicle behavior was obtained during this maneuver, with both longitudinal slip and side-slip angles bounded.

Next, the proposed traction control behavior was evaluated for a sudden acceleration in a curved trajectory, including a change of road friction condition in one side of the vehicle. As it was shown, the proposed strategy ensures the vehicle stability under these conditions.

Finally, the proposed control strategy was verified by changing the tire-road model used in the simulated vehicle. It was shown that even under significant differences in the considered tire model, the proposed traction control system ensures a stable vehicle operation, both in straight and curved trajectories.

APPENDIX A
STABILITY ANALYSIS OF THE PROPOSED OBSERVERS

Consider the lateral dynamics given by (28) and the observer (29), with the estimation error defined as follows,

$$e_v = v - \hat{v}, \tag{41}$$

Besides, the estimation error of the TRFC observers is defined as

$$\mathbf{e}_\zeta = \begin{bmatrix} \zeta_l - \hat{\zeta}_l \\ \zeta_r - \hat{\zeta}_r \end{bmatrix}, \tag{42}$$

with the observers defined in (34). Also, since the TRFC derivative is unknown, assume that the system can be represented as follows,

$$\dot{\zeta}_j = f_j(t), \tag{43}$$

with $j = l, r$. Besides, due to the definition of ζ_j and the physical constraints, it is known that $f_j(t)$ are bounded.

Then, estimation errors dynamics can be expressed as follows,

$$\dot{e}_v = A e_v + \Delta\rho(e_v, \mathbf{e}_\zeta) - g e_v \tag{44}$$

$$\dot{\mathbf{e}}_\zeta = \mathbf{f} - \frac{1}{\epsilon}\mathbf{e}_\zeta. \tag{45}$$

with $\Delta\rho(e_v, \mathbf{e}_\zeta) = \rho(v, \mu_{Sl}, \mu_{Sr}) - \rho(\hat{v}, \hat{\mu}_{Sl}, \hat{\mu}_{Sr})$ and $\mathbf{f} = [f_l \;\; f_r]^T$. Also, we can assume that $\mathbf{f}$ is bounded by some constant value, i.e. $\|\mathbf{f}\| \leq \phi$.

Consider now a candidate Lyapunov function $V_1(\mathbf{e}_\zeta) = \mathbf{e}_\zeta^T \mathbf{P}_1 \mathbf{e}_\zeta$, for the system (45), with $\mathbf{P}_1$ a symmetric positive definite matrix, then

$$\dot{V}_1 = -\frac{2}{\epsilon}\mathbf{e}_\zeta^T \mathbf{P}_1 \mathbf{e}_\zeta + \mathbf{f}^T \mathbf{P}_1 \mathbf{e}_\zeta + \mathbf{e}_\zeta^T \mathbf{P}_1 \mathbf{f}. \tag{46}$$

For simplicity, choose $\mathbf{P}_1 = \mathbf{I}$, so

$$\dot{V}_1 \leq -\frac{2}{\epsilon}\left\|\mathbf{e}_\zeta\right\|^2 + 2\|\mathbf{f}\|\left\|\mathbf{e}_\zeta\right\|. \tag{47}$$

or

$$\dot{V}_1 \leq -\frac{2}{\epsilon}\left\|\mathbf{e}_\zeta\right\|^2 + 2\phi\left\|\mathbf{e}_\zeta\right\|. \tag{48}$$

Then, one can show that [33],

$$\left\|\mathbf{e}_\zeta\right\| \leq \left\|\mathbf{e}_\zeta(0)\right\| \exp\left(-\frac{t}{\epsilon}\right) + \epsilon\phi. \tag{49}$$

As can be seen, the estimation error of ζ_j shows an asymptotic convergence to a final value bounded by $\epsilon\phi$. Thus, the asymptotic error value will be smaller the smaller the value of ϵ.

Convergence of the lateral velocity observer can be analyzed by proposing a candidate Lyapunov function $V_2(e_v) = e_v^2$, with the error dynamics given by (44). In this case,

$$\dot{V}_2 = 2(A - g)e_v^2 + 2\, e_v\, (\Delta\rho(e_v, \mathbf{e}_\zeta)) \tag{50}$$

It can be assumed that $\Delta\rho(e_v, \mathbf{e}_\zeta)$ is bounded by $\left|\Delta\rho(e_v, \mathbf{e}_\zeta)\right| \leq \eta_1 |e_v| + \eta_2 \left\|\mathbf{e}_\zeta\right\|$, with η_1 and η_2 positive constants.

Then,

$$\dot{V}_2 \leq 2(A - g)e_v^2 + 2\eta_1\, e_v^2 + 2\eta_2 |e_v| \left\|\mathbf{e}_\zeta\right\| \tag{51}$$

As shown in (49), $\left\|\mathbf{e}_\zeta\right\|$ is bounded, so it can be assumed a conservative bound as $\left\|\mathbf{e}_\zeta\right\| \leq \Gamma$, so that

$$\dot{V}_2 \leq 2(A - g)e_v^2 + 2\eta_1 e_v^2 + 2\eta_2 \Gamma\, |e_v|\,. \tag{52}$$

and it can be shown that,

$$|e_v| \leq |e_v(0)| \exp(-\sigma t) + \frac{\eta_2 \Gamma}{\sigma} \tag{53}$$

with $\sigma = -(A - g) - \eta_1$. Then, the observer presents asymptotic convergence of the estimation error to an ultimate bound value given by $\frac{\eta_2\Gamma}{\sigma}$. This value depends on the estimation error of $\mathbf{e}_\zeta$ and also on the observer gain g. Besides, σ can be chosen positive by selecting an appropriate value of gain g.

APPENDIX B
DETERMINATION OF A RELIABLE TRFC ESTIMATION

In this section the function $\frac{\partial \hat{F}_{xrj}}{\partial \hat{\mu}_{Sj}}$ obtained from (40) is analyzed to determine the quality of the estimated variables. The expression of this function, now called κ_j, is derived from the force model (3) as follows,

$$\frac{\partial \hat{F}_{xrj}}{\partial \hat{\mu}_{Sj}} = \frac{C^2 R_e \sigma_x \sigma \left(2C\sigma - 9F_{zrj}\mu_{Sj}\right)}{27 I_r F_{zrj}^2 \mu_{Sj}^3} \triangleq \kappa_j \tag{54}$$

Here, the term $(2C\sigma - 9F_{zrj}\mu_{Sj})$ is always negative, because $\sigma <= \sigma_m$ and $\sigma_m = 3\mu_{Sj}F_{zrj}/C$. Therefore the sign of this function only depends on the sign of the longitudinal slip σ_x. By replacing $\sigma = \sqrt{\sigma_x^2 + \sigma_y^2}$ in (54) and by expressing the sideslip as a factor ξ of longitudinal slip ($\sigma_y = \xi\sigma_x$), a scalar function that only depends on σ_x is obtained ($\kappa\ (\sigma_x)$). Then, by taking

$$\frac{\partial \kappa\ (\sigma_x)}{\partial \sigma_x} = 0$$

it is determined that this function has a unique minimum in the range $0 <= \sigma_x <= \sigma_m$, which is located at

$$\sigma_{x\,\min} = \frac{3F_{zrj}\mu_{Sj}\sqrt{1 + \xi^2}}{C(1 + \xi^2)} \tag{55}$$

Because the function $\kappa\ (\sigma_x)$ is always negative, this point corresponds to an absolute maximum of this function. It is interpreted as the point at which the longitudinal force is more dependent of μ_S and it can be demonstrated that at such point the forces are saturated, so $\hat{\mu}_{Sj}$ will be properly estimated. By replacing (55) in (54), the value of κ_j at this point is obtained,

$$\kappa_j\big|_{\sigma_x = \sigma_{x\,\min}} = -\frac{F_{zrj}R_e}{\sqrt{1 + \xi^2}} sign\,(\sigma_x) \triangleq \kappa_{j\,\min} \tag{56}$$

As it can be appreciated, this function is not dependent of the parameter μ_{Sj}. This means that regardless the value of μ_{Sj} estimated by the observer, the minimum of the function can always be calculated from (56) and using F_z, R_e y ξ.

Then, in order to determine the quality of the estimated variables, it is proposed to compare the actual value of κ_j, (54), with a threshold defined here as half of $\kappa_{j\,\min}$,

$$\text{th}_j = \frac{1}{2}\kappa_{j\,\min} = -\frac{1}{2}\frac{F_{zrj}R_e}{\sqrt{1 + \xi^2}}$$

This threshold is used to determine when the longitudinal forces are sufficiently dependent of μ_S, and then assume that the observers are correctly estimating this parameter. Then, traction control would be activated only when ($|\kappa_j| > |\mathrm{th}_j|$), as shown in Fig. 3.

APPENDIX C
ESTIMATION OF THE C PARAMETER IN THE BRUSH MODEL

The proposed estimator is only activated when there is no lateral dynamics ($r = 0$ and $\hat{v}_y = 0$), and when traction forces are in the linear region.

To identify this last situation, an idea similar to the one presented in subsection IV-D is used. There it was assumed that μ_{Sj} is estimated correctly when ($|\kappa_j| > |\mathrm{th}_j|$) because when this condition is met the longitudinal forces are sufficiently dependent of μ_{Sj}. Conversely, in this case we need to know when the longitudinal forces are the linear region. That is, when they are practically independent of μ_{Sj}. For this reason a new limit is defined ($|\kappa_j| < |\mathrm{th}_j|/5$), so the estimator of C only works when this condition is met.

The proposed estimator is based on the vehicle longitudinal dynamics, where the longitudinal acceleration is given by,

$$a_x = \frac{F_{xij} - k_a v_x^2}{m} = \frac{F_{xrl} + F_{xrr} - F_{Rrl} - F_{Rrr} - k_a v_x^2}{m} \quad (57)$$

with k_a a constant parameter which represents the aerodynamic losses, and F_{Rrj} are the rolling resistance forces given by (15).

Since it is assumed that there is no lateral dynamics ($\alpha_{rj} = 0$) and longitudinal slip is very small (in the linear region of forces), the following simplifications can be made:

- forces on the front wheels are neglected by assuming null longitudinal slip;
- normal forces on both rear wheels are equal $F_z = F_{zrl} = F_{zrr}$;
- the tangential velocity in each rear wheel is aproximately equal to the longitudinal vehicle velocity $R_e\omega \approx v_x$.

Therefore, the force model for the rear wheels (3) is approximated as follows,

$$F_{xrj} = C\sigma_{xrj} \quad (58)$$

while the rolling resistance forces can be expressed as,

$$F_{Rrj} = F_z\,(k_s + k_d v_x) \quad (59)$$

Then, (57) can be written as a linear function of the longitudinal slip,

$$\begin{aligned} a_x &= \frac{C}{m}\left(\sigma_{xrj} + \sigma_{xrr}\right) - \frac{k_a v_x^2 + 2F_z\,(k_s + k_d\, v_x)}{m} \\ &= \vartheta\left(\sigma_{xrj} + \sigma_{xrr}\right) + \tau \end{aligned} \quad (60)$$

where τ and ϑ are the coefficients of the linear function.

The following least-squares recursive algorithm is used for estimating the parameters of this linear function,

$$\begin{aligned} K_{[k]} &= \frac{P_{[k]}x_{[k]}}{\lambda + x^T{}_{[k]}P_{[k]}x_{[k]}} \\ P_{[k+1]} &= \left(P_{[k]} - K_{[k]}x^T{}_{[k]}P_{[k]}\right)\frac{1}{\lambda} \\ \hat{\theta}_{[k]} &= \hat{\theta}_{[k-1]} + K_{[k]}\left(y_{[k]} - x^T{}_{[k]}\hat{\theta}_{[k-1]}\right) \end{aligned} \quad (61)$$

where P and K are variables defined by the algorithm, λ the forget factor and

$$\begin{aligned} \hat{\theta}_{[k]} &= \begin{bmatrix} \vartheta \\ \tau \end{bmatrix} \\ y_{[k]} &= a_x \\ x_{[k]} &= \begin{bmatrix} \sigma_{xrj} + \sigma_{xrr} \\ 1 \end{bmatrix} \end{aligned}$$

Longitudinal acceleration, a_x, is measured by an accelerometer. The sampling frequency is 1 kHz and the forgetting factor is set to $\lambda = (1 + 10^{-6})$. The recursive process results in the estimation of the two coefficients of the linear function (ϑ and τ). Then, parameter $\hat{C}$ is obtained as $\hat{C} = \vartheta\, m$.

Parameter τ could be used to estimate or identify the losses that occur in the vehicle due to the resistance of static friction ($2F_z k_s$), dynamic friction ($2F_z k_d v_x$) and aerodynamic losses ($k_a {v_x}^2$), which is considered as a future work.

REFERENCES

[1] L. Serrano-Iribarnegaray and J. Martinez-Roman, "A unified approach to the very fast torque control methods for DC and AC machines," *IEEE Trans. Ind. Electron.*, vol. 54, no. 4, pp. 2047–2056, Aug. 2007.

[2] V. Ivanov, D. Savitski, and B. Shyrokau, "A survey of traction control and antilock braking systems of full electric vehicles with individually controlled electric motors," *IEEE Trans. Veh. Technol.*, vol. 64, no. 9, pp. 3878–3896, Sep. 2015.

[3] Y. Hori, "Future vehicle driven by electricity and control-research on four-wheel-motored 'UOT electric march II,"' *IEEE Trans. Ind. Electron.*, vol. 51, no. 5, pp. 954–962, Oct. 2004.

[4] V. Colli, G. Tomassi, and M. Scarano, "'Single wheel' longitudinal traction control for electric vehicles," *IEEE Trans. Power Electron.*, vol. 21, no. 3, pp. 799–808, May 2006.

[5] G. Xu, K. Xu, C. Zheng, and T. Zahid, "Optimal operation point detection based on force transmitting behavior for wheel slip prevention of electric vehicles," *IEEE Trans. Intell. Transp. Syst.*, vol. 17, no. 2, pp. 481–490, Feb. 2016.

[6] M. Amodeo, A. Ferrara, R. Terzaghi, and C. Vecchio, "Wheel slip control via second-order sliding-mode generation," *IEEE Trans. Intell. Transp. Syst.*, vol. 11, no. 1, pp. 122–131, Mar. 2010.

[7] D. Yin, S. Oh, and Y. Hori, "A novel traction control for EV based on maximum transmissible torque estimation," *IEEE Trans. Ind. Electron.*, vol. 56, no. 6, pp. 2086–2094, Jun. 2009.

[8] G. A. Magallan, C. H. De Angelo, and G. O. Garcia, "Maximization of the traction forces in a 2WD electric vehicle," *IEEE Trans. Veh. Technol.*, vol. 60, no. 2, pp. 369–380, Feb. 2011.

[9] T. Hsiao, "Robust estimation and control of tire traction forces," *IEEE Trans. Veh. Technol.*, vol. 62, no. 3, pp. 1378–1383, Mar. 2013.

[10] R. Rajamani, G. Phanomchoeng, D. Piyabongkarn, and J. Y. Lew, "Algorithms for real-time estimation of individual wheel tire-road friction coefficients," *IEEE/ASME Trans. Mechatronics*, vol. 17, no. 6, pp. 1183–1195, Dec. 2012.

[11] C. Lee, K. Hedrick, and K. Yi, "Real-time slip-based estimation of maximum tire-road friction coefficient," *IEEE/ASME Trans. Mechatronics*, vol. 9, no. 2, pp. 454–458, Jun. 2004.

[12] D. Sui and T. A. Johansen, "Moving horizon estimation for tire-road friction during braking," in *Proc. IEEE Int. Conf. Control Appl. (CCA)*, Sep. 2010, pp. 1379–1384.

[13] C. Ahn, H. Peng, and H. E. Tseng, "Robust estimation of road frictional coefficient," *IEEE Trans. Control Syst. Technol.*, vol. 21, no. 1, pp. 1–13, Jan. 2013.

[14] S. Hong and J. K. Hedrick, "Tire-road friction coefficient estimation with vehicle steering," in *Proc. IEEE Intell. Veh. Symp. (IV)*, Jun. 2013, pp. 1227–1232.

[15] T. Hsiao, "Direct longitudinal tire force control under simultaneous acceleration/deceleration and turning," in *Proc. Amer. Control Conf. (ACC)*, Jun. 2013, pp. 2147–2152.

[16] L. Li, F.-Y. Wang, and Q. Zhou, "Integrated longitudinal and lateral tire/road friction modeling and monitoring for vehicle motion control," *IEEE Trans. Intell. Transp. Syst.*, vol. 7, no. 1, pp. 1–19, Mar. 2006.

[17] G. Baffet, A. Charara, and G. Dherbomez, "An observer of tire–road forces and friction for active security vehicle systems," *IEEE/ASME Trans. Mechatronics*, vol. 12, no. 6, pp. 651–661, Dec. 2007.
[18] G. Baffet, A. Charara, and J. Stephant, "Sideslip angle, lateral tire force and road friction estimation in simulations and experiments," in *Proc. IEEE Int. Conf. Control Appl.*, Oct. 2006, pp. 903–908.
[19] S. Han and K. Huh, "Monitoring system design for lateral vehicle motion," *IEEE Trans. Veh. Technol.*, vol. 60, no. 4, pp. 1394–1403, May 2011.
[20] J. J. Oh and S. B. Choi, "Vehicle velocity observer design using 6-D IMU and multiple-observer approach," *IEEE Trans. Intell. Transp. Syst.*, vol. 13, no. 4, pp. 1865–1879, Dec. 2012.
[21] J.-H. Yoon and H. Peng, "Robust vehicle sideslip angle estimation through a disturbance rejection filter that integrates a magnetometer with GPS," *IEEE Trans. Intell. Transp. Syst.*, vol. 15, no. 1, pp. 191–204, Feb. 2014.
[22] H. Pacejka, *Tire and Vehicle Dynamics*, 2nd ed. New York, NY, USA: Elsevier, 2005.
[23] C. Canudas-de-Wit, P. Tsiotras, E. Velenis, M. Basset, and G. Gissinger, "Dynamic friction models for road/tire longitudinal interaction," *Veh. Syst. Dyn.*, vol. 39, no. 3, pp. 189–226, 2003.
[24] R. Rajamani, *Vehicle Dynamics and Control*. New York, NY, USA: Springer, 2011.
[25] M. Choi, J. J. Oh, and S. B. Choi, "Linearized recursive least squares methods for real–time identification of tire–road friction coefficient," *IEEE Trans. Veh. Technol.*, vol. 62, no. 7, pp. 2906–2918, Sep. 2013.
[26] C. El Tannoury, F. Plestan, S. Moussaoui, and G. P. Gil, "A variable structure observer for an on-line estimation of a tyre rolling resistance and effective radius," in *Proc. 12th Int. Workshop Variable Struct. Syst. (VSS)*, Jan. 2012, pp. 167–172.
[27] W. Cho, J. Yoon, S. Yim, B. Koo, and K. Yi, "Estimation of tire forces for application to vehicle stability control," *IEEE Trans. Veh. Technol.*, vol. 59, no. 2, pp. 638–649, Feb. 2010.
[28] A. N. Atassi and H. K. Khalil, "A separation principle for the stabilization of a class of nonlinear systems," *IEEE Trans. Autom. Control*, vol. 44, no. 9, pp. 1672–1687, Sep. 1999.
[29] H. K. Khalil and L. Praly, "High-gain observers in nonlinear feedback control," *Int. J. Robust Nonlinear Control*, vol. 24, no. 6, pp. 993–1015, Apr. 2014.
[30] J. S. Loeb, D. A. Guenther, H.-H. F. Chen, and J. R. Ellis, "Lateral stiffness, cornering stiffness and relaxation length of the pneumatic tire," SAE Tech. Paper 900129, 1990.
[31] L. Li, K. Yang, G. Jia, X. Ran, J. Song, and Z.-Q. Han, "Comprehensive tire–road friction coefficient estimation based on signal fusion method under complex maneuvering operations," *Mech. Syst. Signal Process.*, vols. 56–57, pp. 259–276, May 2015.
[32] H. B. Pacejka and R. S. Sharp, "Shear force development by pneumatic tyres in steady state conditions: A review of modelling aspects," *Veh. Syst. Dyn.*, vol. 20, nos. 3–4, pp. 121–175, 1991.
[33] J. A. Solsona and M. I. Valla, "Disturbance and nonlinear Luenberger observers for estimating mechanical variables in permanent magnet synchronous motors under mechanical parameters uncertainties," *IEEE Trans. Ind. Electron.*, vol. 50, no. 4, pp. 717–725, Aug. 2003.

Diego A. Aligia (S'12) received the degree in industrial automation and control engineering from the Universidad Nacional de Quilmes, Buenos Aires, Argentina, in 2011, and the Dr.Eng. degree from the Universidad Nacional de Río Cuarto, Río Cuarto, Argentina, in 2017. In 2012, he joined the Grupo de Electrónica Aplicada, Universidad Nacional de Río Cuarto. His research interests include traction control of electric vehicle, electric motor control, no linear estimation, and microcontroller implementation.

Guillermo A. Magallan (S'08–M'10) received the degree in electronic engineering from Universidad Tecnológica Nacional, Paraná, Argentina, in 2002, and the Dr.Eng. degree from the Universidad Nacional de Río Cuarto, Río Cuarto, Argentina, in 2010. In 2005, he joined the Grupo de Electrónica Aplicada, Universidad Nacional de Río Cuarto. His research interests include traction control of electric vehicles, electric motor control, digital-signal processor-based implementation, and power electronics.

Cristian H. De Angelo (S'96–M'05–SM'10) received the degree in electrical engineering from the Universidad Nacional de Río Cuarto, Argentina, in 1999, and the Dr.Eng. degree from the Universidad Nacional de La Plata, Argentina, in 2004. In 1994, he joined the Grupo de Electrónica Aplicada, Universidad Nacional de Río Cuarto, where he is currently an Associate Professor and an Independent Researcher at the Consejo Nacional de Investigaciones Científicas y Técnicas, Argentina. His research interests include electric and hybrid vehicles, fault diagnosis on electric machines, electric motors control, and renewable-energy generation.